Cadmium elicits alterations in mitochondrial morphology and functionality

Oldani M.[a], Manzoni M.[b], Villa A. M.[a], Stefanini F.M.[c], Melchioretto P.[d], Monti E.[b], Forcella M.[a,*], Urani C.[d,e,#], Fusi P.[a,e,#]

[a] *Department of Biotechnology and Biosciences, University of Milano-Bicocca, Piazza della Scienza, 2 - 20126 Milan, Italy*

[b] *Department of Molecular and Translational Medicine (DMTM), University of Brescia, Viale Europa 11, 25123 Brescia, Italy*

[c] *Department of Statistics, Computer Science, Applications, University of Florence, Viale Morgagni 59, 50100 Florence, Italy*

[d] *Department of Earth and Environmental Sciences, University of Milano-Bicocca, Piazza della Scienza 1 - 20126 Milan, Italy*

[e] *Integrated Models for Prevention and Protection in Environmental and Occupational Health, (MISTRAL) University Research Center*

* Corresponding author: Forcella Matilde

E-mail address: matilde.forcella@unimib.it

# these authors are joint senior authors

Highlights

Mitochondria are key targets in cadmium-induced carcinogenicity

Cellular response to cadmium toxicity involves up-regulation of glycolysis

Cadmium inhibits SOD1 activity, raising O_2^- intracellular concentration

Abstract

Background: Cadmium is a widespread contaminant and a recognized carcinogen. We previously showed that the administration of low cadmium doses for 24 hours treatment to healthy C3H10T1/2Cl8 cells at the beginning of Cell Transformation Assay (CTA), up regulates genes involved in metal scavenging and antioxidant defense, like metallothioneines, Glutathione S-transferases and heat shock proteins. Still, although most cells thrive normally in the following weeks, malignancy is triggered by cadmium and leads to *foci* of transformed cells appearance at the end of the CTA. In this work we aim at elucidating the early metabolic deregulation induced by cadmium, underlying healthy cell transformation into malignant cells.

Methods: Respiratory metabolism was investigated through Seahorse Agilent assays in different conditions, while oxidative stress level was assessed through fluorescent probes; DNA damage was evaluated by Comet assay and mitochondrial morphology was analyzed in confocal microscopy.

Results: Results show that, although initial response to cadmium is effective in balancing oxidative stress, through mitochondria rearrangement, SOD1 activity is inhibited, leading to increased O_2^- level, which in turn causes DNA strand breaks. From the metabolic point of view, cells increase their glycolytic flux, although all extra NADH produced is still efficiently reoxidized by mitochondria.

Conclusions: Our results confirm previously shown response against cadmium toxicity; new data about glycolytic increase and mitochondrial rearrangements suggest pathways leading to cell transformation.

General significance: In this work we exploit the widely used, well known CTA, which allows following healthy cells transformation into a malignant phenotype, to understand early events in cadmium-induced carcinogenesis.

Keywords

Cadmium; carcinogenesis; cell metabolism; DNA damage; mitochondria; reactive oxygen species

1. Introduction

Cadmium (Cd) is a toxic heavy metal, normally present in the atmosphere, as a result of gradual erosion and abrasion of rocks and soils [1]. However, since industrialization, it is being massively released into the environment by anthropogenic activities, such as the manufacturing of pigments, stabilizers, alloys, electronic compounds, and especially of rechargeable nickel-cadmium batteries [2].

Human intoxication can take place through inhalation, absorption and ingestion of contaminated water, food and air particles. Apart from professional contact, one of the most widespread routes of exposure is cigarette smoke [3] which contains high amounts of Cd, due to the natural bioaccumulation in tobacco plants. In heavy metal polluted soils, a class of rare plants, called hyper accumulators, are able to accumulate exceptionally high concentrations of trace elements, like Cd, in their aerial parts without visible toxicity symptoms [4].

Acute intoxication causes injuries to the testes, liver and lungs [5], while chronic exposure leads to obstructive airway diseases, emphysema, end-stage renal failures, diabetes and renal complications, deregulated blood pressure, bone disorders and immunosuppression [2] [6].

Therefore, Cd release into the environment, at a current rate of 30000 tons per year, represents a serious threat to human health.

Cadmium is also a group I carcinogen, recognized by the International Agency for Research on Cancer [7]. Its oncogenic potential can be assessed through the *in vitro* Cell Transformation Assay (CTA), a valuable tool for carcinogenicity evaluation and mechanistic studies in fundamental research and in the regulatory context, in an integrated approach to testing and assessment [8]. Despite many studies on Cd toxicity, its pathogenic mechanism leading to cancer is still not fully elucidated. Cd similarity to zinc (Zn) has led to propose a “Trojan horse” mechanism of toxicity, in which Cd could enter the cells through Zn transporters and potentially substitute this essential metal in the nearly 3800 different Zn proteins in living cells.

Aging and many diseases including cancer, are related to malfunctioning of mitochondria [9]. These are dynamic organelles with highly variable shape and size, existing as large networks or as discrete organelles according to the predominance within the cell of either fusion or fission [10] [11]. Cells with a high fusion to fission ratio contain few highly interconnected long shaped mitochondria [12]; conversely, cells with a low fusion to fission ratio have numerous fragmented mitochondria appearing as small spheres and/or short rods [11]. Metals, like manganese, iron, copper, and zinc play essential roles as cofactors in mitochondria, helping mitochondrial proteins functions in processes such as electron transfer and enzymatic catalysis. Since the overall concentration of metal ions in mitochondria is finely regulated by metallochaperones and metal transporters [13], any imbalance in metal homeostasis can lead to mitochondrial function impairment. In particular, an increase in Zn cytoplasmic concentration has been shown to impair tricarboxylic acid cycle through alpha-ketoglutarate dehydrogenase inhibition [14]. Moreover, redox-inactive Zn(II) hampers the proton transfer to ubiquinone and the proton translocation across the inner mitochondrial membrane by blocking the proton channels in complex I [15].

Mitochondria are the key intracellular targets for different stressors including Cd [16], but the mechanisms of metal-induced mitochondrial damage are still not fully understood. Moreover, Cd has previously been shown to trigger ROS production at the mitochondrial level and eventually lead to cell death, caused by severe mitochondrial dysfunction [17] [18].

In a previous work [19] we have used the CTA as a tool to study the pathogenetic mechanisms underlying Cd carcinogenicity, through a toxicogenomics approach. Exposure of C3H10T1/2Cl8 cells to Cd at non-cytotoxic concentrations ($<IC_{50}$) for 24 hours switched a series of detoxifying mechanisms such as up-regulation of metallothioneins, scavenging glutathione S-transferase (GSTα) and different members of the heat shock proteins (HSPs) family. However, although the cells seem to thrive healthily in the following recovery weeks of culture, after 4-6 weeks colonies of transformed cells (*foci*) inevitably appear, thus showing that Cd injuries were also present in apparently healthy cells.

In the search of mechanisms accounting for the biological effects leading to *foci* formation, we turned to early events triggered by Cd and in particular we focused on mitochondria as possible targets. In this study, we investigate the effect of 24 hours Cd administration to C3H10T1/2Cl8 healthy cells. We chose C3H cells since they are used in the widely accepted *in vitro* CTA for chemical carcinogenesis assessment. Cadmium was administered for 24 hours in order to observe early effects and at low doses to mimic chronic exposure, which is closer to the conditions of human exposure to environmental contaminants. Cadmium was added to cultured cells at 1 μM $CdCl_2$ concentration, which had previously been established to induce cell transformation and *foci* generation [20]. However, experiments were also performed with 4 μM $CdCl_2$, in order to assess whether some effects, which were repeatedly observed at 1 μM but without statistical significance, were actually caused by Cd administration. Moreover, $CdCl_2$ supplementation for 24

hours allowed comparison of the observed metabolic effects with data of a previous toxicogenomics study [19].

Our aim is the identification of early key events running in the powerhouses of the cells, triggering the carcinogenic transformation of the few cells that escape the multiple defense mechanisms.

2. Materials and methods

2.1 Cell and culture conditions

The experiments were performed using contact-sensitive C3H10T1/2 clone 8 (C3H from here on) mouse embryonic fibroblasts (cell line ATCC, CCL 226 lot. n. 58078542). These cells were chosen for their high sensitivity to carcinogenic compounds, their low spontaneous transformation rates, and the fact that are among the cell lines suggested to perform the Cell Transformation Assays [21]. Cells were stored in ampoules, frozen at –80 °C with 10% sterile DMSO as preservative. Cells were cultured in Basal Medium Eagle (BME, Sigma Chemical Co., St. Louis, MO) enriched with 10% heat-inactivated fetal bovine serum (FBS, EuroClone, Pero, Italy), 1% glutamine, 0.5% HEPES 2M and 25 µg/mL gentamicin (all from Sigma) at 37 °C in a humidified incubator supplied with a constant flow of 5% CO_2 in air throughout each experiment. Cells were routinely seeded in 100 mm Ø Petri dishes, the medium was changed every 3 days and cells grown until 80% confluence maximum was reached.

2.2 Detection of Intracellular Reactive Oxygen Species (ROS)

The generation of intracellular reactive oxygen species (ROS) was detected by the oxidation of 2',7'-Dichlorofluorescin diacetate (H_2DCFDA) or Dihydroethidium (DHE). H_2DCFDA is an indicator for both reactive oxygen species and nitric oxide (•NO); the second probe measures the level of cytosolic superoxide anion (O_2^-). The cells were plated at a density of 2.5 x 10^5 cells per well into six-well plates in complete culture medium. The day after the seeding, the cells were exposed to 1 or 4 µM $CdCl_2$ for 24 hours, by changing the normal medium with a medium enriched with $CdCl_2$. At the end of the treatment, cells were incubated with H_2DCFDA (5 µM final concentration in PBS) or DHE (10 µM final concentration in complete medium) for 20 min in the dark at 37 °C. At the end of incubation, cells were washed by warm PBS, trypsinized (500 µl of trypsin /well) and harvested by centrifugation (5 min at 2000 *g*) at room temperature. The pellet was resuspended in 500 µl/tube of PBD and ROS generation of 10.000 cells was measured by the fluorescence intensity. FL-1 channel (530 nm) was utilized to detect the fluorescence intensity of DCF; DHE fluorescence can be measured at 585 nm, or FL-2 channel, band-pass filter. Logarithmic amplification was used to detect probe fluorescence. Flowcytometric data were analyzed using CytExpert 2.3 Software (Beckman Coulter, Inc.).

2.3 Enzymatic assays

For enzymatic assay sample preparation, the cells were seeded at 1 × 10^6 cells/100 mm dish and 24 hours after seeding were exposed to 1 or 4 µM $CdCl_2$ for 24 hours, by changing the medium with a $CdCl_2$ enriched medium. The $CdCl_2$ stock solution (1 mM, 97% purity BDH Laboratory, Milan, Italy) was prepared in ultra-pure water (0.22 µm filtered Milli-Q water, Millipore, Vimodrone, Milan, Italy) and stored at 4 °C. Previous experiments performed by our group [22] [20]

demonstrated that 1 μM $CdCl_2$ is able to induce the formation of transformed colonies of cancerous cells (*foci*) in the Cell Transformation Assay.

Cells were then rinsed with ice-cold PBS and lysed in 50 mM Tris/HCl 50, pH 7.4, 150 mM NaCl, 5 mM EDTA, 10 % glycerol, 1 % NP40 buffer, containing protease inhibitors and 1mM PMSF. After lysis on ice, homogenates were obtained by passing the cells 5 times through a blunt 20-gauge needle fitted to a syringe and then centrifuging at 15,000 *g* for 30 min at 4°C. The resulting supernatant was used to measure enzymatic activities. Enzymes were assayed using the following procedures. Lactate dehydrogenase (LDH) and gliceraldeide-3-phosphate dehydrogenase (GAPDH) were assayed according to [23] (1974); catalase (CAT) was assayed according to [24], using 12 mM H_2O_2 as substrate; glutathione-S-transferase (GST) as reported in Habig et al. [25]; glutathione peroxidase according to [26]; glutathione reductase according to Wang [27]. For superoxide dismutase1 (SOD1) cells were rinsed with ice-cold PBS and lysed in PBS, containing protease inhibitors and 1mM PMSF. After lysis on ice, homogenates were obtained by passing the cells 5 times through a blunt 20-gauge needle fitted to a syringe, incubating on ice for 15 min and sonicating 2 times (10 s cycle). The supernatant was obtained by centrifugation at 15,000 *g* for 10 min at 4°C and used to measure enzymatic activities according to [28]. All assays were performed in triplicate at 30 °C in a Cary3 Spectrophotometer and analyzed by the Cary Win UV application software for Windows. Activity was expressed in international units and referred to protein concentration as determined by the Bradford method [29].

2.4 Glutathione detection

Cells were plated at a density of 1 x 10^6 cells/100 mm dish in complete culture medium. The day after seeding, the cells were exposed to 1 or 4 μM $CdCl_2$ for 24 hours, by changing the normal

medium with a $CdCl_2$ enriched medium. At the end of the treatment, the cells were trypsinized and harvested by centrifugation at room temperature, for 10 min at 1200 *g*. The pellet was resuspended in 3 mL PBS, harvested by a centrifugation in the above conditions and weighted. Pellets were resuspended in 500 µl cold 5% 5-sulfosalicylic acid (SSA), lysed by vortexing and by passing 5 times through a blunt 20-gauge needle fitted to a syringe. All the samples were incubated for 10 minutes at 4 °C and then centrifuged at 14.000 *g* for 10 minutes at 4 °C. The supernatant was used for the analysis following the instructions of Glutathione Colorimetric Detection Kit (Invitrogen). The Kit is designed to measure oxidized glutathione (GSSG), total glutathione (GSH tot) and reduced glutathione (GSH tot – GSSG) concentrations. Therefore, it was possible to obtain GSH/GSSG ratio, a critical indicator of cell health. The absorbance was measured at 405 nm using a micro plate reader. The values of absorbance were compared to standard curves (GSH tot and GSSG, respectively) and normalized to mg of cells. Final concentrations were expressed in nmol/mg cells.

2.5 Comet Assay

Single Cell gel electrophoresis (SCGE) or Comet assay is a microgel electrophoresis technique to assess DNA damage at single cells level. The protocol under alkaline conditions (pH >13) allows to measure single and double-strand breaks, incomplete repair sites and alkali-labile sites. The procedure started with the degreasing of microscope slides and the preparation of 0.65% w/v normal melting point (NMPA) and 0.5% w/v low melting point agarose (LMPA) in PBS. A minimum of two slides are prepared and maintained at 4°C for every single sample in each experiment and pre-coated with NMPA the day before the experiments. The cells were seeded at a density of 1.65 x 10^5 cells/100 mm dish in complete culture medium. The day after seeding, the cells were

exposed to 1 or 4 µM $CdCl_2$ for 24 hours. At the end of the treatment, the cells were trypsinized and harvested by centrifugation for 10 minutes at 1200 *g* at room temperature. Pellets were resuspended in 900 µl LMPA and 100 µl of this suspension was dropped on the solidified NMPA. A cover slip was placed over the gel and the slides solidified at 4°C for 10-15 min. The procedure was repeated with another layer of LMPA. Subsequently, in a darkroom, the cover slips were removed and the slides were covered with a cold lysis solution (2.5 M NaCl, 100mM Na_2EDTA, 10mM Tris/HCl, 300 mM NaOH, 1% Triton and 10% DMSO at pH 10) for 1 hour, placing them in the electrophoresis system. The slides were dipped in cold alkaline buffer (300 mM of NaOH and 1mM of EDTA) for 15 min in order to unwind DNA strands. Electrophoresis was carried out for 15 min at 0.8 V/cm. The slides were treated with neutralizing buffer (400 mM Tris/HCl pH 7.5) for 10 min; 20 µL of DAPI staining solution were dropped on the slides. Alongside each experiment, cells treated with 50 µM H_2O_2 for 30 minutes were considered as positive control. Three biological replicates were performed. To visualize the stained slides, a Zeiss fluorescent microscope equipped with an excitation filter of 515-560 nm, with a barrier filter of 590 nm and a magnification of 200X, was used. About 30 cells for each treatment and for controls were analyzed with the Comet Imager 1.2.14 (MetaSystems) program. Four parameters were measured, as indicative of DNA damage: Tail Length (TL), %Tail DNA, Tail Moment (TM) and Olive Tail Moment (OTM) [30]. TL and %Tail DNA are able to quantify the extent of DNA damage; while TM, or rather OTM are considered to be particularly useful in describing heterogeneity within a cell population, as OTM can emphasize variations in DNA distribution within the tail.

2.6 *Oxygen consumption rate and extra-cellular acidification rate measurements*

Oxygen consumption rate (OCR) and extra-cellular acidification rate (ECAR) were measured in adherent C3H fibroblasts with Seahorse XFe24 Analyzer (Seahorse Bioscience, Billerica, MA, USA) using Seahorse XF Cell Mito Stress Test Kit and Agilent Seahorse XF Glycolytic Rate Assay Kit. The cells were seeded in Agilent Seahorse XF24 cell culture microplates at density of 30×10^3 cells/well in 250 µL of Basal Medium Eagle and 24 hours after seeding were exposed to 1 or 4 µM $CdCl_2$ for 24 hours.

The day of the assay the growth medium was replaced with 525 µl/well of Seahorse XF Base Medium containing 1 mM pyruvate, 2 mM glutamine and 10 mM glucose for the Cell Mito Stress Test Kit or 1 mM pyruvate, 2 mM glutamine, 10 mM glucose and 5 mM Hepes for the Glycolytic Rate Assay Kit. Then the plate was incubated into 37°C non-CO_2 incubator for 1 h, before starting the experiment procedure.

The sensor cartridge was calibrated by Seahorse XFe24 Analyzer. Pre-warmed Oligomycin, FCCP, Rotenone and Antimycin A were loaded into injector ports A, B and C of sensor cartridge, to reach working concentration of 1 µM, 2 µM and 0.5 µM respectively, for the Cell Mito Stress Test Kit. Pre-warmed Rotenone and Antimycin A and 2-deoxy-D-glucose (2-DG) were loaded into injector ports A and B of sensor cartridge, to reach working concentration of 0.5 µM and 50 mM for the Glycolytic Rate Assay Kit.

OCR and ECAR were detected under basal conditions followed by the sequential addition of the drugs, to measure non-mitochondrial respiration, maximal respiration, proton leak, ATP respiration, respiratory capacity, coupling efficiency for the Cell Mito Stress Test Kit and basal glycolysis, basal proton efflux rate, compensatory glycolysis and post 2-DG acidification for the Glycolytic Rate Assay Kit.

2.7 Mitochondrial transmembrane potential (MTP) assay

MTP alterations were assessed flowcytometrically, using the potentially sensitive dye 3,3' - dihexyloxacarbocyanine Iodide. The cells were plated at a density of 2.5 x 10^5 cells per well into six-well plates in complete culture medium. The day after the seeding, the cells were exposed to 1 or 4 μM $CdCl_2$ for 24 hours, by changing the normal medium with a medium enriched with $CdCl_2$. At the end of the treatment the cells were harvested by centrifugation (5 min at 2000 *g*) at room temperature and stained with DiOC6 (40 nM in PBS, 20 min at 37 °C and 5% CO_2 in the dark). Loss in DiOC6 fluorescence indicates disruption of the mitochondrial inner transmembrane potential. The probe was excited at 488 nm and emission was measured through a 530 nm (FL-1 channel) band-pass filter. Logarithmic amplification was used to detect the fluorescence of the probe. Flowcytometric data were analyzed using CytExpert 2.3 Software (Beckman Coulter, Inc.).

2.8 Confocal microscopy

Mitochondria fluorescence in living cells was studied by laser scanning confocal microscopy, using a Bio-Rad MRC-600 confocal microscope equipped with a 25mW argon laser (Bio-Rad, Hemel Hempstead, UK). The scanning head was coupled with an upright epifluorescence microscope Nikon Optiphot-2 (Nikon, Tokyo, Japan) with a 60x oil immersion objective Nikon Planapochromat (N.A. = 1.4).

For R123 staining, the cells were plated in 35mm Petri dishes at a density of 6 x 10^4 cells and left to grow for 24 hours in culture medium. Then $CdCl_2$ was added to the medium to a final concentration of 1 or 4 μM $CdCl_2$. After 24 hours, the medium was removed, cells were washed twice with phosphate buffer saline (PBS) and incubated for 10 min in 1 μM Rhodamine 123 (R123) solution at 37 °C and 5% CO_2. After incubation, the cells were rinsed twice with PBS and few

microliters of PBS were left in the Petri dish to avoid cell drying. A coverslip was placed over the cells that were immediately imaged by confocal microscope.

R123 fluorescence was excited at 488 nm and the emission collected through a long pass filter above 515 nm. High sensitivity photon counting detection was used to minimize the excitation power (0.1mW at the entry of the optical head) and preserve cell viability.

2.9 Images analysis

Original confocal microscope images in a TIFF format were imported into R after loading the EBimage R package [31]. We developed original R code using the EBimage application programming interface to segment each image into a number of regions of interests (ROIs), where a ROI refers to a cell nucleus and its surrounding regions populated by mitochondria. If two ROIs overlapped then they were excluded, together with their nuclei, from the analysis. Grey levels were normalized after estimating the average background by collecting pixel intensities well outside ROIs. At the end of the procedure, distances of each pixel from the center of the cell nucleus within each ROI were also stored (measurement unit: number of pixels) for further analysis. The algorithm produced a PDF file for each processed image in which every intermediate image was stored to allow visual inspection of each processing step. All elaborations were performed using the R software and the following packages: *ggplot2, EBimage, coin, RVAideMemoire* [32-35] [31].

The average distance of pixels (ADP) from nucleus was calculated for each ROI in three different experimental conditions: control cells, 1 μM $CdCl_2$, 4 μM $CdCl_2$. Statistical tests were performed to evaluate changes in the distribution of ADP under the three experimental conditions.

2.10 *Statistical analysis*

The distributions of ADP obtained from confocal microscope images under CD treatment were compared to the control treatment using the Kolgomorov-Smirnov nonparametric test [36]. The hypotheses were refined by Mood's median test for the equality of medians.

In all other experiments, samples were compared to their reference controls and the data were tested by Dunnett multiple comparison procedure. All calculations were conducted using the R software environment for statistical computing and graphics [32].

3. Results

3.1 Cadmium treatment increases the production of superoxide anion

Previous reports of cadmium mediated increase in cellular reactive oxygen species (ROS) production [17] prompted us to evaluate ROS content in Cd treated healthy C3H cells. Total cytoplasmic ROS were evaluated with cytoflex, using H_2DCFDA fluorescent probe, while superoxide anion (O_2^-) was assessed through DHE fluorescent probe. Measurements of DCF fluorescence, reported in Fig. 1 showed that the overall ROS production decreased following $CdCl_2$ administration and that this reduction is more evident in cells treated with 4μM $CdCl_2$ (p value < 0.01) than in cells treated with 1 μM $CdCl_2$. On the other hand, DHE fluorescence was found higher in cells treated with 4 μM $CdCl_2$ (p value < 0.05), showing that this metal induces a remarkable increase in the production of superoxide anion (Fig. 2).

The activity of the enzymes involved in keeping oxidative stress under control was also assayed. Fig. 3A shows the results of activity assays of Glutathione-S-transferase (GST), Glutathione reductase (GR), Glutathione peroxidase (GPox), catalase (CAT) and superoxide dismutase 1 (SOD1).

While both GST and GR activities were found to increase significantly upon treatment with 4 µM $CdCl_2$, catalase activity was found to be reduced following the same treatment. Interestingly, SOD1 activity was diminished following treatment with both 1 and 4 µM $CdCl_2$, thus likely accounting for the increase in superoxide anion concentration. The increase in GR and GST was paralleled by an increase in total cell glutathione in 4 µM $CdCl_2$ treated samples, as shown in Fig. 3B. However, the ratio between oxidized (GSSG) and reduced glutathione (GSH) remained constant in all conditions.

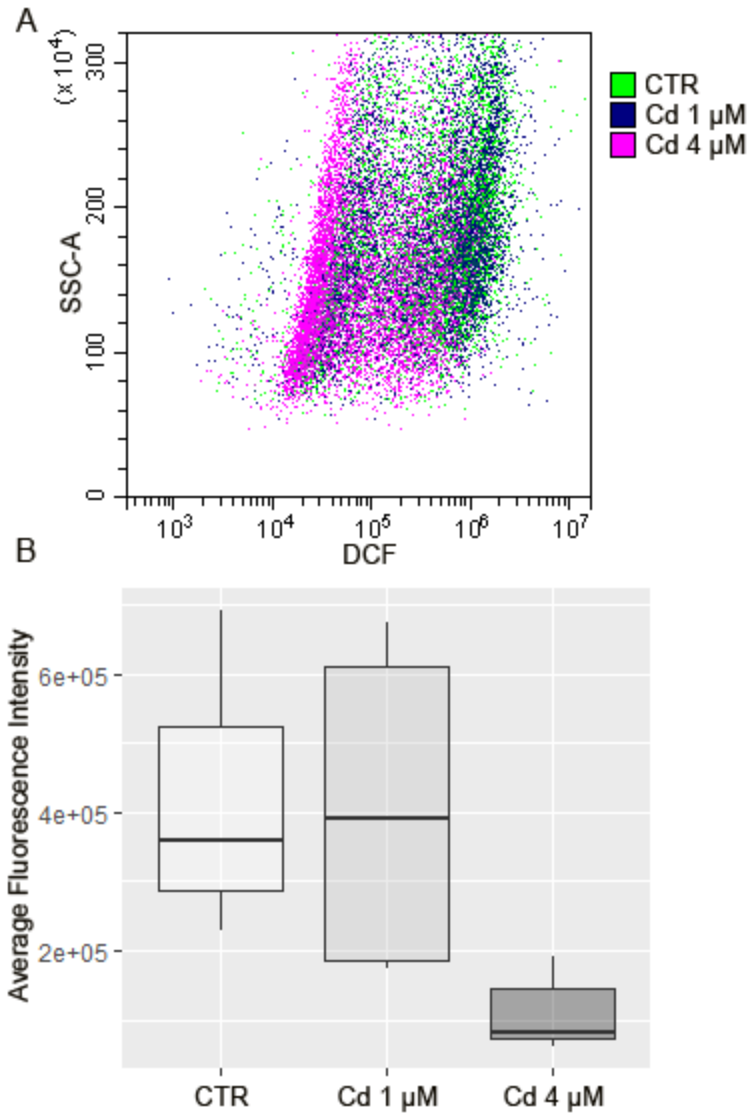

Fig. 1. Flowcytometric analysis of cadmium–induced ROS production in C3H cells. A) Cells are exposed to 1 or 4 µM of cadmium chloride for 24 hours. After the treatment, cells are incubated

with 5 µM H2DCFDA and the level of fluorescence of treated-cells is compared to the controls. The results are shown in a dot plot overlay. The dot plot is representative of three independent experiments. B) The fluorescence intensity of all experiments is represented by a box plot. The dark line within a box represents the median value, while the upper and lower sides of a box are the third and first quartiles, respectively. Statistical significance Cd 4µM vs CTR: ** $p < 0.01$ (Dunnett's test).

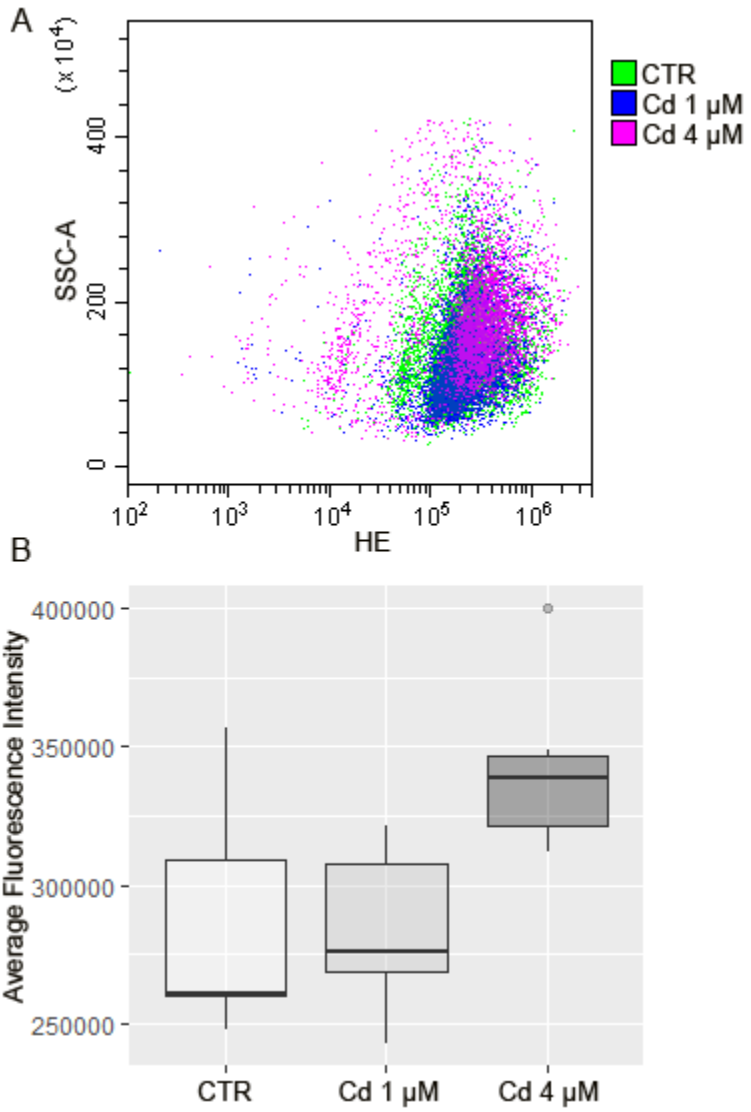

Fig. 2. Flowcytometric analysis of cadmium–induced superoxide anion production in C3H cells. A) Cells are exposed to 1 or 4 µM of cadmium chloride for 24 hours. After the treatment, cells are

incubated with 10 µM DHE and the level of fluorescence of treated-cells is compared to the controls. The results are shown in a dot plot overlay. The dot plot is representative of three independent experiments. B) The dark line within a box represents the median value, while the upper and lower sides of a box are the third and first quartiles, respectively. Statistical significance Cd 4µM vs CTR: * $p < 0.05$ (Dunnett's test).

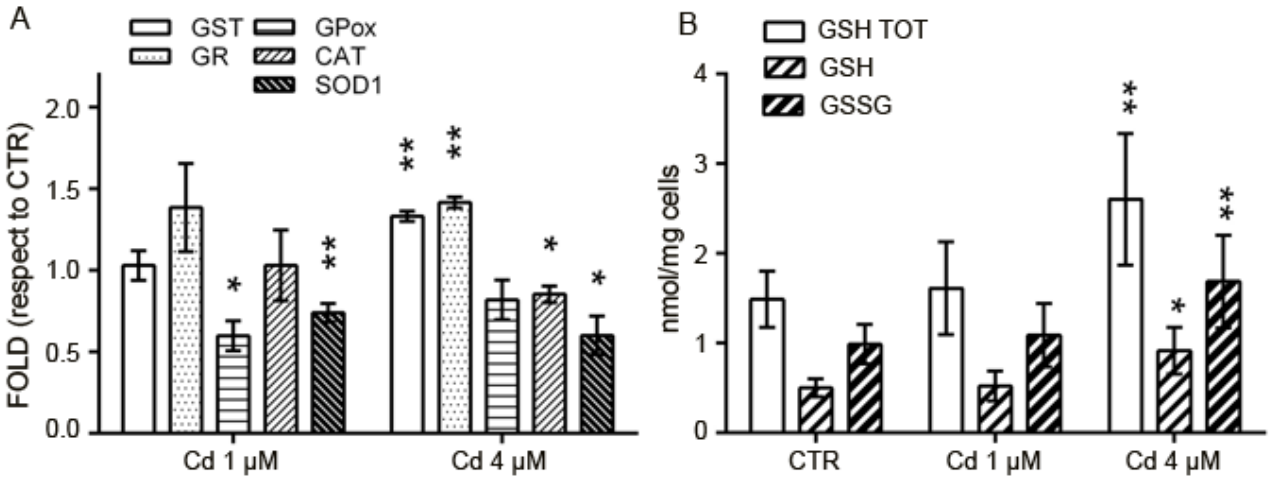

Fig. 3. A) Enzymatic analysis in C3H cells exposed to 1 µM or 4 µM of cadmium chloride for 24 hours. The results are expressed as fold respect to untreated controls and are shown as mean ± SEM from three independent experiments. B) Glutathione level in C3H cells exposed to 1 µM or 4 µM of cadmium chloride for 24 hours. The results are expressed in µM and normalized respect to mg of cells. Statistical significance: * $p < 0.05$, ** $p < 0.01$ (Dunnett's test).

3.2 Comet assay reveals damage to nuclear DNA upon cadmium treatment

Although Cd is a non-genotoxic metal, it has been reported to damage DNA in an indirect way, through ROS production [37]. O_2^- is recognized as the most effective ROS in inducing DNA damage, as well as the only ROS overproduced in our $CdCl_2$-treated cells; this prompted us to evaluate

cadmium effect on nuclear DNA by Comet assay. Microscopy results obtained after treatment with 1 or 4 μM $CdCl_2$ for 24 hours are shown in Fig. 4. DNA integrity from untreated control cells appears as a sun (Fig. 4A, left), while DNA of cells treated with 4 μM $CdCl_2$ appear as a comet (Fig. 4A, right), with DNA fragments in the so called tail region of the comet. Image analysis (Fig. 4B) showed that both the tail length and the percent DNA in tail were significantly increased in cells treated with cadmium. In particular, the first value increases fourfold after 4 μM $CdCl_2$ treatment while the percent DNA in tail gets triple respect to control cells. The lowest cadmium concentration shows all parameters comparable to those of controls, thus revealing non-significant DNA damage. H_2O_2 treated cells, as expected by this positive control, show highly statistical values ($p<0.001$ Dunnett's test) of all parameters analyzed indicative of an extended DNA damage.

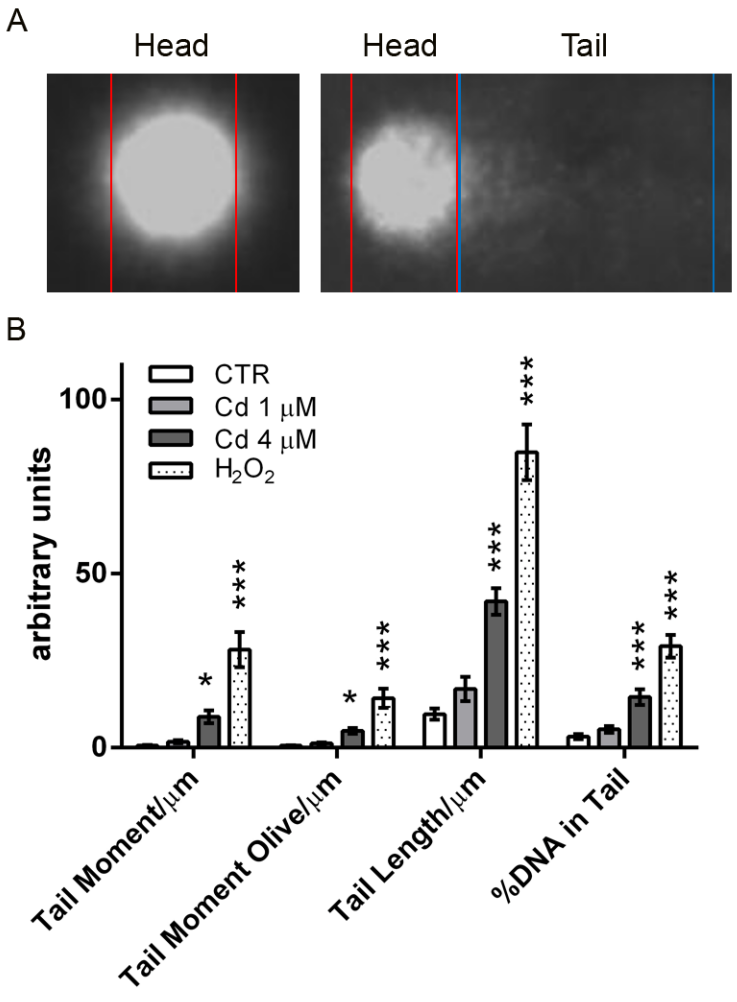

Fig. 4. COMET assay for DNA damage evaluation in C3H cells exposed to 1 μM or 4 μM of cadmium chloride for 24 hours. A) Image of a sun (on the left) corresponding to typical undamaged control cells, and of a comet (on the right), stained with DAPI and detected by fluorescent microscopy. B) Analysis of different parameters for DNA damage quantification. Bars indicate the mean ± SEM of parameters in thirty cells analyzed for each sample condition, representative of three independent experiments. Statistical significance: * $p < 0.05$, *** $p < 0.001$ (Dunnett's test).

3.3 Mitochondria of cadmium treated cells show altered metabolism, with increased membrane potential

Respiratory metabolism was investigated measuring oxygen consumption rate (OCR), basal respiration, spare respiratory capacity, ATP synthesis and extracellular acidification rate (ECAR), through Agilent Seahorse analyses. Results are shown in Fig. 5: treatment with cadmium increased both basal respiration and spare respiratory capacity, although both parameters were found significantly increased only after treatment with 4 μM $CdCl_2$ (Fig. 5A, B and C). Moreover, the increase in spare respiratory capacity following 4 μM $CdCl_2$ treatment far exceeded the increase in basal respiration, suggesting a higher availability of oxidable substrates. ATP production (Fig. 5C) was also increased upon treatment with $CdCl_2$, although to a significant extent only in cells treated with 4 μM $CdCl_2$. ECAR measurement (Fig. 5D) revealed that cells treated with 4 μM $CdCl_2$ showed a higher level of acidification during basal respiration, which was not affected by ATPase inhibition. Since both treated and untreated cells showed fully coupled mitochondria (Fig. 5E), this stronger acidification seems to be due to glycolysis rather than to CO_2 produced by oxidative phosphorylation. Fig. 5D also shows that ECAR increase upon FCCP addition and mitochondria uncoupling was much higher 4 μM $CdCl_2$ treated cells than in untreated cells, again suggesting that

it may be due to increased glycolysis. Moreover, after rotenone addition and electron transport inhibition, ECAR did not decrease to untreated cells level, confirming a substantial contribute of glycolysis. Moreover, all these rearrangements in oxidative phosphorylation were found perfectly reversible (data not shown) upon cadmium removal, after a period of recovery of 24 hours.

In accordance with Seahorse results, $\Delta\psi$, measured with cytoflex using DiOC6 fluorescent probe, was found to be increased (more negative) in cadmium treated cells. As shown in Fig. 6, cells treated with 1 μM $CdCl_2$ showed increased DiOc6 fluorescence, indicative of a more negative $\Delta\Psi$, increase that was even more marked in cells treated with 4 μM $CdCl_2$ (p value < 0.05).

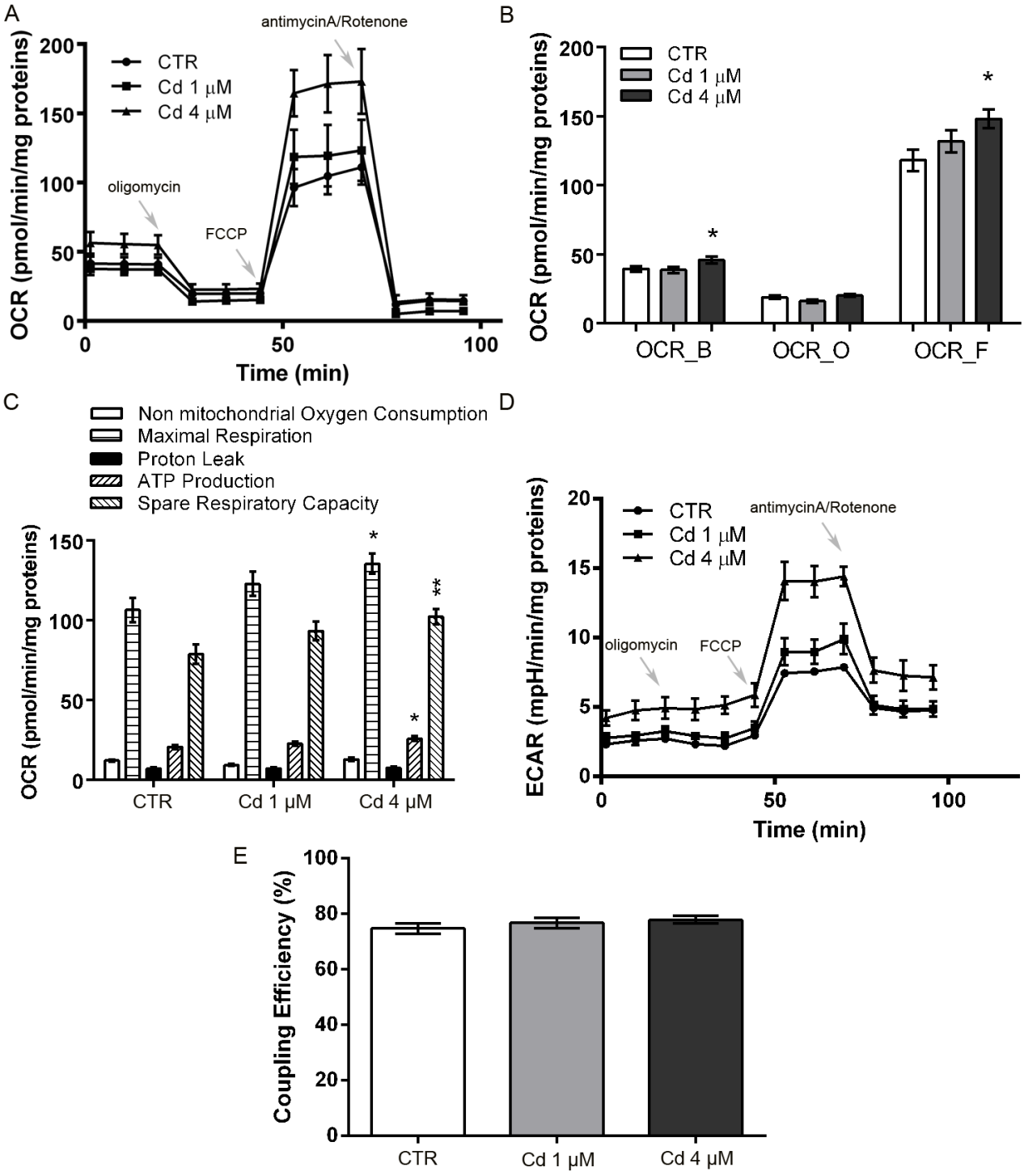

Fig. 5. Seahorse mitostress analysis in C3H cells exposed to 1 µM or 4 µM of cadmium chloride for 24 hours. A) OCR traces, expressed as pmoles O2/min/mg proteins in control and Cd-treated C3H cells. The arrows indicate the time of oligomycin, FCCP and antimycinA/rotenone addiction. The OCR profile is representative of three independent experiments. B) The values at points 3, 6, 9 reflect OCR_B (basal), OCR_O (oligomycin) and OCR_F (FCCP). Bars indicate the mean ± SEM

obtained in three independent experiments. C) Analysis of different parameters related with mitochondrial function. D) ECAR traces, expressed as mpH/min/mg proteins, in control and Cd-treated C3H cells. The arrows indicate the time of oligomycin, FCCP and antimycinA/Rotenone addiction. The ECAR profile is representative of three independent experiments. E) Coupling efficiency. Statistical significance: * $p < 0.05$, ** $p < 0.01$ (Dunnett's test).

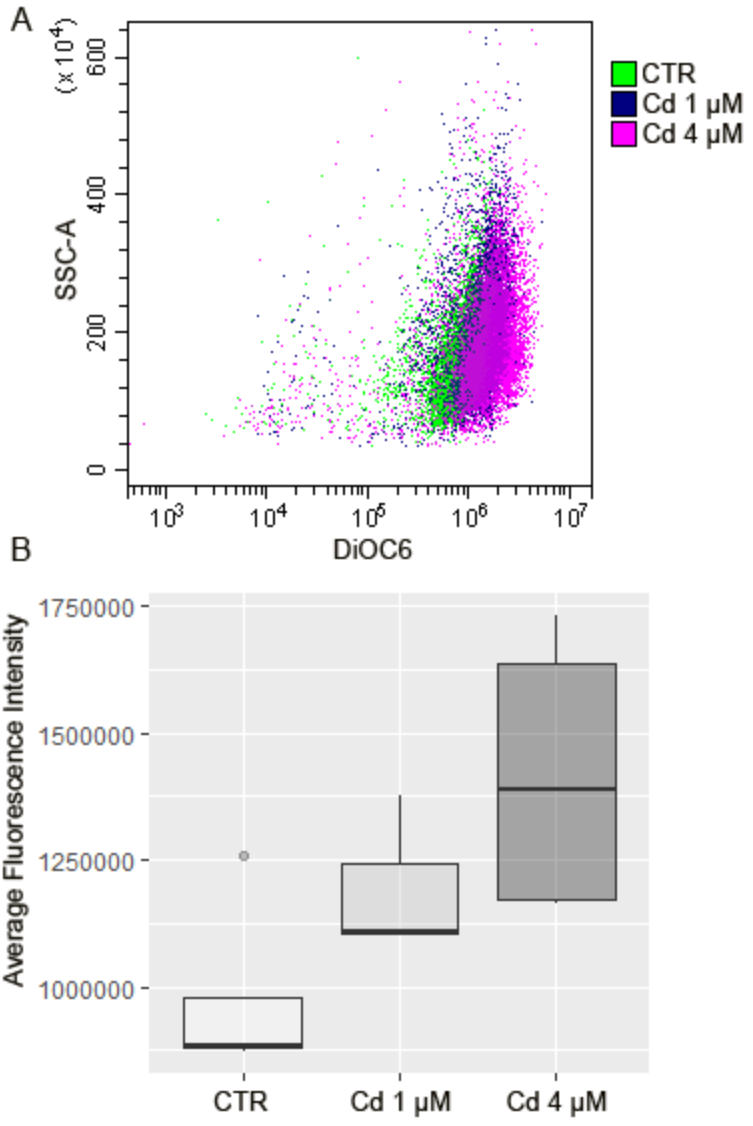

Fig. 6. Flowcytometric analysis of mitochondrial Δψ in C3H cells. A) Cells are exposed to 1 or 4 µM of cadmium chloride for 24 hours. After treatment, the cells are incubated with 40 nM DiOC6 and the level of fluorescence of treated-cells is compared to the controls. The results are shown in a

dot plot overlay. The results are representative of three independent experiments. B) The fluorescence intensity of all experiments is represented by a box plot. The dark line within a box represents the median value, while the upper and lower sides of a box are the third and first quartiles, respectively. Statistical significance Cd 4μM vs CTR: * $p < 0.05$ (Dunnett's test).

3.4 Cadmium treated mitochondria show increased glycolysis

Glycolytic contribution to extracellular acidification rate was determined through Seahorse, using the Glycolytic Assay kit (Fig. 7). In both control and 4 μM $CdCl_2$ treated cells, the proton efflux rate (PER) was found to be sustained by mitochondrial electron transport as well as by glycolysis, to almost the same extent. However, upon addition of rotenone and antimicin A, inhibiting complex III, cells treated with 4 μM $CdCl_2$ showed a higher glycolytic compensation, thus confirming a higher glycolytic capacity, accounting for the higher spare respiratory capacity (Fig. 7B). The addition of hexokinase inhibitor 2-deoxyglucose (2-DG) completely abolished PER (Fig. 7A). However, neither lactate nor lactate dehydrogenase activities were significantly increased in our experiments (Fig. 7C), suggesting that the higher glycolytic compensation shown by 4 μM $CdCl_2$ treated cells is obtained by a higher glycolytic NADH production.

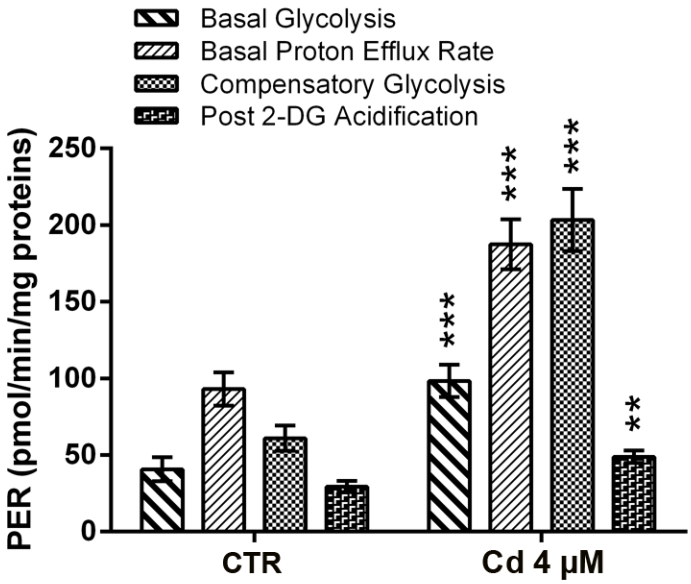

Fig. 7. Seahorse glycolytic analysis in C3H cells exposed to 4 µM of cadmium chloride for 24 hours. Analysis of different parameters related with glycolysis. Bars indicate the mean ± SEM obtained in three independent experiments. Statistical significance: ** $p < 0.01$, *** $p < 0.001$ (Student's t-test).

3.5 Confocal microscopy shows an altered morphology and intracellular distribution of mitochondria upon treatment with cadmium

Confocal microscopy images of living control and $CdCl_2$ treated cells stained with R123 were collected to investigate mitochondria morphology and intracellular distribution.

As seen in Fig. 8A, mitochondria in control cells are distributed through the cytoplasm and extend from the nucleus to the cell periphery. When considering the only feature of mitochondria distribution within the cells, a similar intracellular localization is observed at 1 µM $CdCl_2$ for 24 hours (Fig. 8B), while cells treated with 4 µM $CdCl_2$ for 24 hours (Fig. 8C) show mitochondria mainly crowded in the perinuclear region, with only sparse organelles at the cytoplasm periphery.

Enlarged views of Fig. 8A, 8B, and 8C allow to appreciate the details of mitochondria morphology. In control cells (Fig. 8A, inset 1, 2, 4), mitochondria are mainly filamentous and elongated, sometimes showing rod-like shape (Fig. 8A, inset 3). These elongated and well-separated mitochondria are organized in wide networks.

In contrast, in 1 μM $CdCl_2$ treated cells (Fig. 8B) mitochondria mainly show a less elongated shape, sometimes giving rise to a very dense network (Fig. 8B, inset 1) or presenting a swollen morphology (Fig. 8B, insets 2, 3), an indication of damaged organelles.

In 4 μM $CdCl_2$ treated cells, (Fig. 8C) the crowding of mitochondria in the perinuclear region does not allow to appreciate their morphology (Fig. 8C, insets 1, 2, 4). At the cell periphery, punctate and rod-like shaped mitochondria are observed (Fig. 8C, inset 3).

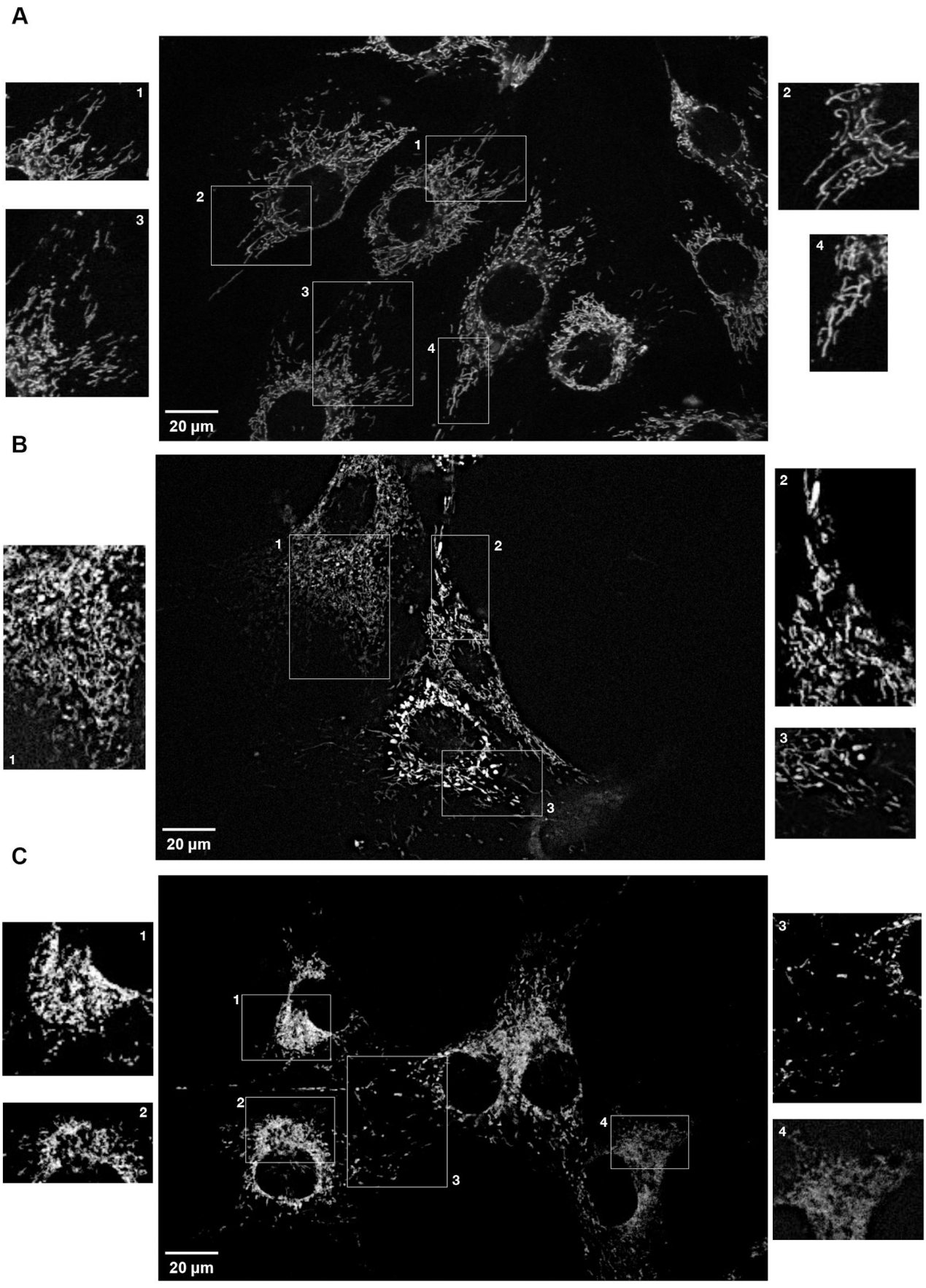
A
1
2
3
4
20 µm
B
1
2
3
20 µm
C
1
2
3
4
20 µm

Fig. 8. Representative confocal images of: A) C3H control cells with the typical mitochondrial network organization and filamentous features; B) C3H cells treated with 1 μM $CdCl_2$ for 24 hours, showing altered dense network and swollen morphology and C) C3H cells treated with 4 μM $CdCl_2$ for 24 hours showing a crowding of mitochondria in the perinuclear region. Enlarged views allow to appreciate the details of these morphological features.

The average distances of pixels from cell nucleus (ADP), acquired in the first step of the digital image analysis, were summarized using a boxplot for each treatment, as reported in Fig. 9. The median, the first and the third quartiles of ADP were expressed in microns.

Figure 9 also shows the presence of extreme values, in particular in control and 4 μM $CdCl_2$ treated cells, we therefore preferred the median to the mean for its well-known robustness with respect to the presence of candidate outlying observations. For this reason, we also preferred to perform statistical tests for the distribution of ADP and for the equality of medians, without taking the Normal distribution as a reference.

The Kolgomorov-Smirnov tests [36] for the equality of probability distribution functions (cdfs, indicated as F) were performed on the ADP variable under different treatments: if cadmium has an effect then empirical distributions of ADP have to show (partially) different features over treatments. Both control cells vs 1 μM $CdCl_2$ and control vs 4 μM $CdCl_2$ comparisons were found statistically significant, with p-values of 0.0350 and 0.0267 respectively.

We also calculated the Bonferroni adjustment for multiple testing to protect the resulting three tests against false nulls rejection: the resulting working alpha value was 0.0166, thus after test protection the null hypotheses were not rejected anymore.

Mood median test for the refined hypothesis of median equality was performed and the p value of the test statistic comparing three medians was 0.0635 (control cells vs 1 μM $CdCl_2$, control vs 4 μM $CdCl_2$, as well as 1 μM $CdCl_2$ vs 4 μM $CdCl_2$).

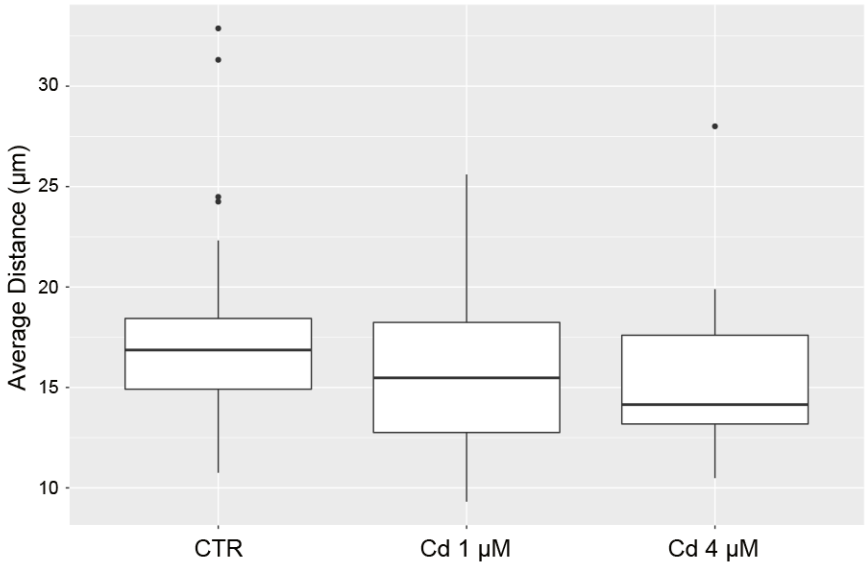

Fig. 9. Boxplots of average distance values. The distribution of ADP (average distance of pixels from cell nucleus), converted in μm, is summarized by one boxplot for each treatment. The dark line within a box represents the median value, while the upper and lower sides of a box are the third and first quartiles, respectively. The so-called whiskers outside the box extend to 1.5 times the interquartile range from the box. Observations outside the two whiskers are considered candidate outliers with respect to a normal distribution.

4. Discussion

In contrast to what believed in the past, recent epidemiological studies have provided numerous evidence that even low-level environmental exposure to cadmium, nowadays occurring in numerous economically developed countries, represents a risk for the health of the general population [38]. In particular, the study of cadmium carcinogenic mechanism is of the outmost

importance, due to the fact that this heavy metal does not undergo biodegradation in the environment and limitation of exposure to this toxic metal is very difficult.

The information gathered over the past decades has strengthened the role of the mitochondria in normal physiology and in pathology. In particular, tumorigenesis *per se* was shown as a mitochondrial disease where metabolically hijacked mitochondria become highly dependent on glucose and glutamine [39], while oxidative metabolism antagonizes metastasis [40].

With the aim of understanding intracellular early effects of low doses of cadmium, which eventually trigger cell transformation, we turned to the study of oxidative stress and defense mechanism, as well as mitochondria morphology and metabolism.

Assessment of total ROS, estimated through H_2DCFDA fluorescent probe, showed an overall decrease in ROS content following cadmium administration. Although this may seem at first surprising, ROS have been shown to possess dual functions. Actually, low levels of ROS can activate various signaling pathways that stimulate cell proliferation and survival, whereas excess ROS irreversibly damage cellular macromolecular components (proteins, lipids, nucleic acids) and cause cell death (including apoptosis) [40]. In both healthy and pathological conditions, mitochondria generate ROS, which act as signaling and/or damaging molecules, in a hormetic way. In particular, ROS have been shown to regulate mitochondrial dynamics through acting on mitochondrial fusion and fission proteins, permitting (auto)regulation of mitochondrial morphology and function by redox-mediated signaling [41]. In our experiments, cadmium induced higher basal mitochondrial respiration, as well as increased $\Delta\psi$, ATP production and mitochondrial spare respiratory capacity, suggesting an overall improved mitochondrial metabolic efficiency. Moreover, no difference in mitochondrial coupling between electron transport and ATP synthesis was observed following cadmium administration. This overall higher efficiency of mitochondrial respiration can be related to the change in morphology and subcellular localization, as observed

by confocal microscopy, with mitochondria more densely packed around the nuclei in cadmium treated cells, so that a more efficient network can be realized, despite the occurrence of some mitochondria damage, as suggested by the presence of swollen mitochondria. Mitochondria perinuclear localization has been previously observed in many cancer cells [42]. Moreover, accumulating evidence suggests that cellular and mitochondrial redox homeostasis is linked to mitochondrial dynamics. This has led to the novel concept of ‘‘mitochondrial morphofunction”, a tight and multidirectional connection between mitochondrial internal structure, external structure, and function, although a comprehensive understanding is currently still lacking [43]. Moreover, mitochondria have an intrinsic ability to sense their state of health and, when stressed, induce compensatory quality-control mechanisms, such as fusion or fission and mitophagy of damaged mitochondria. Normally, high oxidative phosphorylation activity correlates with mitochondrial fusion and is consistent with the proposal that elongated mitochondrial networks are more efficient at energy generation. Increased ATP production also leads to fusion, with uncoupling leading to fusion inhibition [44]. However, in diseases such as cancer, mitochondria phenotypes have been shown to vary between tumors, showing a predominant punctuate (spherical), network or swollen morphology, and can be used to classify types of cancer [45]. Very similarly to what we observed, Giedt et al. [45] reported that, after 0.1 mM selenium administration, morphology of lung A459 cells showed a progressive shift from a networked to a punctuate and finally to a swollen phenotype. Swollen mitochondria were also observed *in vivo* in renal cortex [46] and in liver [47] of rats treated with cadmium·

Although cadmium has been reported to increase ROS in many previous studies, the overall reduction in ROS content observed in our experiments is likely due to the efficient response against oxidative stress induced by cadmium. This is confirmed by the increase of glutathione reductase activity, as well as of total cell glutathione. The increase in GST activity is also part of this

defense mechanism, although this enzyme is more likely to be endowed with a scavenger role towards cadmium, as previously highlighted by toxicogenomic data [19]. The reason why cadmium administration leads to an increase in GR activity probably lies in the fact that cytosolic SOD1 and peroxisomal catalase, which are primarily involved in O_2^- detoxification, are less active, so that ROS detoxification is mainly achieved through glutathione. Both SOD1 and catalase are metalloenzymes, the former containing Zn and Cu in the catalytic site, the latter only Cu. The ability of cadmium to interfere with essential bioelements such as zinc, magnesium, selenium, calcium, and iron resulting in alteration of their homeostasis and disturbance in their biological functions has been well documented [48]. Prolonged low-level exposure to cadmium has been reported to decrease the activity of antioxidative enzymes (SOD1 and catalase) and the concentration of non-enzymatic antioxidants (reduced glutathione, –SH groups, vitamin C and E) in the liver, leading to the oxidative damage to the hepatocytes [9].

Although the overall ROS content was found diminished, the evaluation of superoxide anion (O_2^-) showed that production of this ROS was significantly enhanced by 4 μM $CdCl_2$ administration, thus confirming the impaired ability to remove O_2^- caused by SOD1 and catalase partial inactivation. Interestingly, O_2^- accumulation leads to some extent of DNA fragmentation, which might be responsible for irreversible cell damage and could also account for the fraction of swollen mitochondria that are seen in confocal images of cells treated with 4 μM $CdCl_2$. The DNA damage observed and consequent genomic instability could contribute to the formation of transformed and cancerous *foci* from the cells able to escape the repair and protection mechanisms. In fact, it is reported that cadmium is able to impair almost all major DNA repair pathways and that this effect is likely due to inactivation of enzyme and tumor suppressors functions [37] [49] [50] [51].

Zinc is easily displaced by cadmium, from all zinc proteins, including the zinc buffering proteins, metallothioneines [52] [37] and this can alter zinc intracellular homeostasis. Interestingly, a study

performed on neuronal cell cultures highlighted mitochondria as targets of Zn^{2+} [53]. These authors reported that upon loading of neocortical mice primary cultures with 300 μM $ZnCl_2$ (a condition which occurs during ischemia), cytosolic Zn^{2+} can enter mitochondria and induce effects including loss of mitochondrial membrane potential, mitochondrial swelling, and ROS generation. Since cadmium addition is known to displace zinc from zinc-proteins, the effect we observe in C3H cells can be partially mediated by zinc release, a condition previously observed in C3H cells and human hepatoma cells [19] [52]. However, comparing our experiments with those reported by Ji and Weiss [53], the main difference lies in the concentrations of zinc used by the authors which cannot possibly be equaled by those of zinc released by 1 or 4 μM $CdCl_2$ used in our experiments. These concentrations still lie in a range where efficient defense mechanisms are available, so that we do not observe mitochondrial network disruption, but rather an increase in mitochondria efficiency. However, we do observe mitochondrial swelling, which could lead to irreversible damage, should cadmium persist in the medium. Mitochondrial impairment, reported by Belyaeva and colleagues [17], is also likely caused by the high $CdCl_2$ doses (500 μM) used by these authors.

Our results show that cells respond to cadmium treatment with an increase in $\Delta\psi$; although this can seem at first in contrast with other studies showing that cadmium induces mitochondrial damage involving a decrease in $\Delta\psi$ [17] [54], it can be explained by the low cadmium doses we have used, which allow the cells to build up an effective defense, and is in accordance with the overall frame of improved oxidative phosphorylation, revealed by Seahorse assays. In fact, a previous study [54], performed on hepatocytes, showed that $CdCl_2$ reduced ATP production as well as $\Delta\psi$ in a time-dependent manner. In addition to mitochondrial dysfunction, cell viability also underwent a time-dependent reduction. However, the $CdCl_2$ concentration of 12 μM used by the authors in hepatic cells is much higher than in our experiments and expected to lead to irreversible cell damages.

Taking a closer look at mitochondrial oxidative phosphorylation, our results show that, besides increased basal OCR and spare respiratory capacity, 4 μM $CdCl_2$ treatment induces an ECAR increase upon FCCP addition, which is due to increased proton pumping following increased electron transport rate, but also upon electron transport inhibition through rotenone and antimycin A. The latter can only be due to increased glycolysis, as it is also demonstrated by the measure of proton efflux rate (PER): during basal respiration, PER is maintained by both mitochondrial CO_2 production and glycolytic acidification, in both control and 4 μM $CdCl_2$ treated cells. However, when oxidative phosphorylation is inhibited, cadmium treated cells show an increase in PER, due to a higher glycolytic compensatory capacity, as shown by the fact that it is abolished by 2-DG addition. This increase in glycolysis, sustaining both higher extracellular acidification and increased respiratory capacity, must yield more NADH, which can be oxidized by the electron transport chain to yield more ATP.

5. Conclusions

Our work shows that low doses of $CdCl_2$ trigger cells to increase the glycolytic flux, without increasing lactate production. NADH is effectively shuttled to mitochondria, where it can be oxidized, its removal from the cytosol preventing glycolysis inhibition. Still, as NADH increasingly accumulates, lactate production is likely to be activated. Moreover, increased NADH could lead to decreased histones deacetylation, which is linked to higher cell proliferation.

On the whole, what we see in our cells is an efficient defense mechanism against moderate cadmium concentrations, which upon cadmium removal or inactivation by binding to defense proteins (e.g., metallothioneines, MTs) allows most cells to grow normally, although, only a very few become transformed and give rise fully transformed *foci*, at the end of the CTA [20]. What we

see is likely still a reversible condition: with the help of an efficient detoxification by MTs and GSTs, as previously detected [19], and despite O_2^- increased generation, if cadmium is administered at low doses and removed and/or inactivated by protein chelation after 24 hours, most cells can regain their healthy state. However, there are a few metabolic rearrangements, triggered by cadmium, which may become irreversible in a small number of cells and lead to transformation and *foci* formation; these rearrangements include increased glycolysis, O_2^- production and induced DNA damages, and mitochondrial impairment. Taken together, our results show how mitochondria represent key targets of this carcinogenic toxic metal. However, further studies will be necessary to establish the direct link between all the observed morpho-functional alterations and the induction of cell transformation.

Funding

This work was supported by the University of Florence (*Progetto Dipartimenti di Eccellenza*" - MIUR, Italy, 2018-2022, FMS); by the University of Milano-Bicocca (grants 2017-ATE-0335 to CU and 2017-ATE-0273 to PF).

Author contributions

Oldani Monica: Formal analysis, Investigation, Data curation; writing-review & editing; **Manzoni Marta**: Investigation, writing-review & editing; **Villa Anna Maria**: Investigation, Writing-original draft, writing-review & editing; **Stefanini Federico Mattia**: Software, Formal analysis, Resources, Funding acquisition, writing-review & editing; **Melchioretto Pasquale**: Investigation, writing-review & editing; **Monti Eugenio**: Resources, writing-review & editing; **Urani Chiara**:

Conceptualization, Resources, Writing-original draft, Funding acquisition, writing-review & editing; **Fusi Paola**: Conceptualization, Resources, Writing-original draft, Funding acquisition, writing-review & editing; **Forcella Matilde**: Conceptualization, Validation, Writing-original draft, Supervision, writing-review & editing.

References

[1] L.B. Marcano, I.M. Carruyo, X.M. Montiel, C.B. Morales, P.M. de Soto, Effect of cadmium on cellular viability in two species of microalgae (Scenedesmus sp. and Dunaliella viridis), Biol Trace Elem Res, 130 (2009) 86-93.

[2] L. Jarup, A. Akesson, Current status of cadmium as an environmental health problem, Toxicol Appl Pharmacol, 238 (2009) 201-208.

[3] P. Richter, O. Faroon, R.S. Pappas, Cadmium and Cadmium/Zinc Ratios and Tobacco-Related Morbidities, Int J Environ Res Public Health, 14 (2017).

[4] U. Kramer, Metal hyperaccumulation in plants, Annu Rev Plant Biol, 61 (2010) 517-534.

[5] S. Kakuta, S. Shibata, Y. Iwakura, Genomic structure of the mouse 2',5'-oligoadenylate synthetase gene family, J Interferon Cytokine Res, 22 (2002) 981-993.

[6] T. Jin, Q. Kong, T. Ye, X. Wu, G.F. Nordberg, Renal dysfunction of cadmium-exposed workers residing in a cadmium-polluted environment, Biometals, 17 (2004) 513-518.

[7] IARC, TOXICOLOGICAL PROFILE FOR CADMIUM, U.S. Department of Health and Human Services, Public Health Service Agency for Toxic
Substances and Disease Registry, (2012).

[8] R. Corvi, M.J. Aardema, L. Gribaldo, M. Hayashi, S. Hoffmann, L. Schechtman, P. Vanparys, ECVAM prevalidation study on in vitro cell transformation assays: general outline and conclusions of the study, Mutat Res, 744 (2012) 12-19.

[9] G. Cannino, E. Ferruggia, C. Luparello, A.M. Rinaldi, Cadmium and mitochondria, Mitochondrion, 9 (2009) 377-384.

[10] H. Chen, D.C. Chan, Mitochondrial Dynamics in Regulating the Unique Phenotypes of Cancer and Stem Cells, Cell Metab, 26 (2017) 39-48.

[11] S.A. Detmer, D.C. Chan, Functions and dysfunctions of mitochondrial dynamics, Nat Rev Mol Cell Biol, 8 (2007) 870-879.

[12] E. Smirnova, L. Griparic, D.L. Shurland, A.M. van der Bliek, Dynamin-related protein Drp1 is required for mitochondrial division in mammalian cells, Mol Biol Cell, 12 (2001) 2245-2256.

[13] P.A. Lindahl, M.J. Moore, Labile Low-Molecular-Mass Metal Complexes in Mitochondria: Trials and Tribulations of a Burgeoning Field, Biochemistry, 55 (2016) 4140-4153.

[14] A.M. Brown, B.S. Kristal, M.S. Effron, A.I. Shestopalov, P.A. Ullucci, K.F. Sheu, J.P. Blass, A.J. Cooper, Zn2+ inhibits alpha-ketoglutarate-stimulated mitochondrial respiration and the isolated alpha-ketoglutarate dehydrogenase complex, J Biol Chem, 275 (2000) 13441-13447.

[15] M. Schulte, D. Mattay, S. Kriegel, P. Hellwig, T. Friedrich, Inhibition of Escherichia coli respiratory complex I by Zn(2+), Biochemistry, 53 (2014) 6332-6339.

[16] B. Sanni, K. Williams, E.P. Sokolov, I.M. Sokolova, Effects of acclimation temperature and cadmium exposure on mitochondrial aconitase and LON protease from a model marine ectotherm, Crassostrea virginica, Comp Biochem Physiol C Toxicol Pharmacol, 147 (2008) 101-112.
[17] E.A. Belyaeva, D. Dymkowska, M.R. Wieckowski, L. Wojtczak, Reactive oxygen species produced by the mitochondrial respiratory chain are involved in Cd2+-induced injury of rat ascites hepatoma AS-30D cells, Biochim Biophys Acta, 1757 (2006) 1568-1574.
[18] S. Nemmiche, Oxidative Signaling Response to Cadmium Exposure, Toxicol Sci, 156 (2017) 4-10.
[19] G. Callegaro, M. Forcella, P. Melchioretto, A. Frattini, L. Gribaldo, P. Fusi, M. Fabbri, C. Urani, Toxicogenomics applied to in vitro Cell Transformation Assay reveals mechanisms of early response to cadmium, Toxicol In Vitro, 48 (2018) 232-243.
[20] M. Forcella, G. Callegaro, P. Melchioretto, L. Gribaldo, M. Frattini, F.M. Stefanini, P. Fusi, C. Urani, Cadmium-transformed cells in the in vitro cell transformation assay reveal different proliferative behaviours and activated pathways, Toxicol In Vitro, 36 (2016) 71-80.
[21] OECD, Detailed review paper on cell transformation assays for detection of chemical carcinogens, Development, O.f.e.c.-o.a. (Ed). OECD Environment, health and safety publications, (2007) 1-164.
[22] C. Urani, F.M. Stefanini, L. Bussinelli, P. Melchioretto, G.F. Crosta, Image analysis and automatic classification of transformed foci, J Microsc, 234 (2009) 269-279.
[23] G.K. Bergmeyer HU, Grassl M. , Enzymes as biochemical reagents, in: B. HU (Ed.) Methods of enzymatic analysis, vol. 1, Academic Press, New York, 1974, pp. 427-522.
[24] G.M. Bergmeyer HU, Enzymes. Catalase, in: B. HU (Ed.) Methods of enzymatic analysis, vol. 2, New York: Academic Press, NewYork, 1983, pp. 165-166.
[25] W.H. Habig, M.J. Pabst, W.B. Jakoby, Glutathione S-transferases. The first enzymatic step in mercapturic acid formation, J Biol Chem, 249 (1974) 7130-7139.
[26] H.S. Nakamura W, Hayashi K. , Purification and properties of rat liver glutathione peroxidase, Biochim Biophys Acta, 358 (1974) 251-261.
[27] Y. Wang, L.W. Oberley, D.W. Murhammer, Antioxidant defense systems of two lipidopteran insect cell lines, Free Radic Biol Med, 30 (2001) 1254-1262.
[28] P.G. Vance, B.B. Keele, Jr., K.V. Rajagopalan, Superoxide dismutase from Streptococcus mutans. Isolation and characterization of two forms of the enzyme, J Biol Chem, 247 (1972) 4782-4786.
[29] M.M. Bradford, A rapid and sensitive method for the quantitation of microgram quantities of protein utilizing the principle of protein-dye binding, Anal Biochem, 72 (1976) 248-254.
[30] T.S. Kumaravel, A.N. Jha, Reliable Comet assay measurements for detecting DNA damage induced by ionising radiation and chemicals, Mutat Res, 605 (2006) 7-16.
[31] G. Pau, F. Fuchs, O. Sklyar, M. Boutros, W. Huber, EBImage--an R package for image processing with applications to cellular phenotypes, Bioinformatics, 26 (2010) 979-981.
[32] R.C. Team, R: A language and environment for statistical computing. , R Foundation for Statistical Computing Vienna, Austria, (2008).
[33] W. H, ggplot2: Elegant Graphics for Data Analysis, (2016).
[34] K.H. Torsten Hothorn, Mark A. van de Wiel, Achim Zeileis Implementing a Class of Permutation Tests: The coin Package, Journal of Statistical Software 28(8) (2008) 1-23.
[35] R.D.M.M. Hervé, Testing and Plotting Procedures for Biostatistics, (2018).
[36] P.H. Kvam, Non parametric statistic with applications to science and engineering, Wiley, 2007.
[37] A. Hartwig, Cadmium and cancer, Met Ions Life Sci, 11 (2013) 491-507.

[38] M. Mezynska, M.M. Brzoska, Environmental exposure to cadmium-a risk for health of the general population in industrialized countries and preventive strategies, Environ Sci Pollut Res Int, 25 (2018) 3211-3232.
[39] M. Neagu, C. Constantin, I.D. Popescu, D. Zipeto, G. Tzanakakis, D. Nikitovic, C. Fenga, C.A. Stratakis, D.A. Spandidos, A.M. Tsatsakis, Inflammation and Metabolism in Cancer Cell-Mitochondria Key Player, Front Oncol, 9 (2019) 348.
[40] J. Lu, M. Tan, Q. Cai, The Warburg effect in tumor progression: mitochondrial oxidative metabolism as an anti-metastasis mechanism, Cancer Lett, 356 (2015) 156-164.
[41] W. Mayer, M. Hemberger, H.G. Frank, R. Grummer, E. Winterhager, P. Kaufmann, R. Fundele, Expression of the imprinted genes MEST/Mest in human and murine placenta suggests a role in angiogenesis, Dev Dyn, 217 (2000) 1-10.
[42] L.W. Thomas, O. Staples, M. Turmaine, M. Ashcroft, CHCHD4 Regulates Intracellular Oxygenation and Perinuclear Distribution of Mitochondria, Front Oncol, 7 (2017) 71.
[43] E.P. Bulthuis, M.J.W. Adjobo-Hermans, P. Willems, W.J.H. Koopman, Mitochondrial Morphofunction in Mammalian Cells, Antioxid Redox Signal, 30 (2019) 2066-2109.
[44] P. Mishra, D.C. Chan, Metabolic regulation of mitochondrial dynamics, J Cell Biol, 212 (2016) 379-387.
[45] R.J. Giedt, P. Fumene Feruglio, D. Pathania, K.S. Yang, A. Kilcoyne, C. Vinegoni, T.J. Mitchison, R. Weissleder, Computational imaging reveals mitochondrial morphology as a biomarker of cancer phenotype and drug response, Sci Rep, 6 (2016) 32985.
[46] W. Tang, Z.A. Shaikh, Renal cortical mitochondrial dysfunction upon cadmium metallothionein administration to Sprague-Dawley rats, J Toxicol Environ Health A, 63 (2001) 221-235.
[47] J.O. Ossola, M.L. Tomaro, Heme oxygenase induction by cadmium chloride: evidence for oxidative stress involvement, Toxicology, 104 (1995) 141-147.
[48] B. Messner, A. Turkcan, C. Ploner, G. Laufer, D. Bernhard, Cadmium overkill: autophagy, apoptosis and necrosis signalling in endothelial cells exposed to cadmium, Cell Mol Life Sci, 73 (2016) 1699-1713.
[49] A. Hartwig, M. Asmuss, H. Blessing, S. Hoffmann, G. Jahnke, S. Khandelwal, A. Pelzer, A. Burkle, Interference by toxic metal ions with zinc-dependent proteins involved in maintaining genomic stability, Food Chem Toxicol, 40 (2002) 1179-1184.
[50] C. Urani, P. Melchioretto, M. Fabbri, G. Bowe, E. Maserati, L. Gribaldo, Cadmium Impairs p53 Activity in HepG2 Cells, ISRN Toxicol, 2014 (2014) 976428.
[51] T. Fatur, T.T. Lah, M. Filipic, Cadmium inhibits repair of UV-, methyl methanesulfonate- and N-methyl-N-nitrosourea-induced DNA damage in Chinese hamster ovary cells, Mutat Res, 529 (2003) 109-116.
[52] C. Urani, P. Melchioretto, M. Bruschi, M. Fabbri, M.G. Sacco, L. Gribaldo, Impact of Cadmium on Intracellular Zinc Levels in HepG2 Cells: Quantitative Evaluations and Molecular Effects, Biomed Res Int, 2015 (2015) 949514.
[53] S.G. Ji, J.H. Weiss, Zn(2+)-induced disruption of neuronal mitochondrial function: Synergism with Ca(2+), critical dependence upon cytosolic Zn(2+) buffering, and contributions to neuronal injury, Exp Neurol, 302 (2018) 181-195.
[54] S. Xu, H. Pi, Y. Chen, N. Zhang, P. Guo, Y. Lu, M. He, J. Xie, M. Zhong, Y. Zhang, Z. Yu, Z. Zhou, Cadmium induced Drp1-dependent mitochondrial fragmentation by disturbing calcium homeostasis in its hepatotoxicity, Cell Death Dis, 4 (2013) e540.